Electronic Supplementary Information

Synergistic Engineering of Architecture and Composition in $Ni_xCo_{1-x}MoO_4$@$CoMoO_4$ Nanobrush Arrays towards Efficient Overall Water Splitting Electrocatalysis

Zekun Li, [a] Mingyue Zheng, [b] Xian Zhao, [b] Jun Yang [c] and Weiliu Fan *[a]

a. School of Chemistry and Chemical Engineering, Shandong University, Jinan 250100, China.

b. State Key Laboratory of Crystal Materials, Shandong University, Jinan 250100, China.

c. Institute of Process Engineering, Chinese Academy of Sciences, Beijing 100190, China.

*E-mail: fwl@sdu.edu.cn

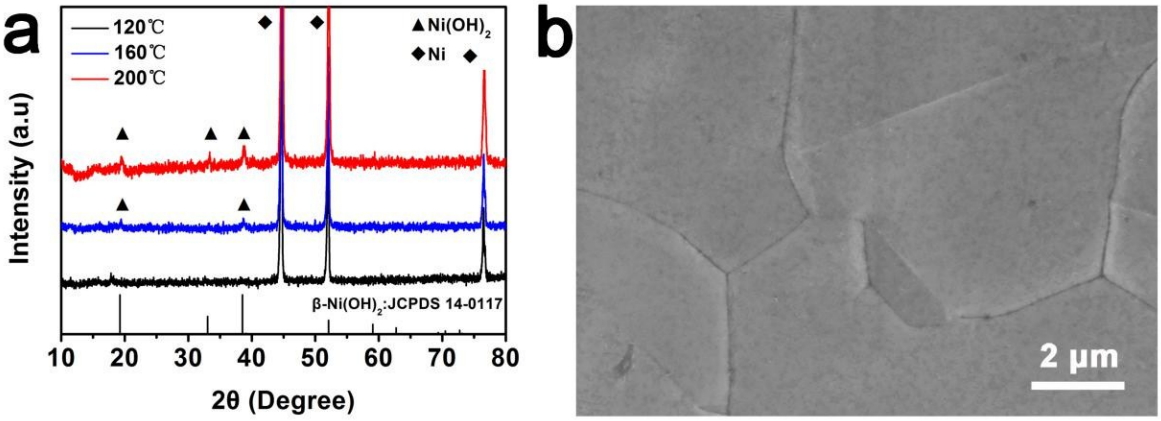

Figure S1. (a) XRD patterns for act-NF-120 ˚C, act-NF-160 ˚C and act-NF-200 ˚C, respectively; and (b) the SEM images of bare NF.

the bare NF has three strong peaks in its XRD pattern, which are at 41.5°, 51.8° and 76.3°, corresponding to the (111), (200) and (220) planes of Ni respectively (JCPDS NO. 04-0850). There is no other peak observed in the XRD pattern for act-NF prepared at 120 ℃. When the preparation temperature is 160 ℃, two weak and broad peaks at 19.2° and

38.5° appear, representing diffraction from the (001) and (101) planes of β-$Ni(OH)_2$ (JCPDS NO. 14-0117). When the synthetic temperature is 200 ℃, a new peak at 33°, corresponding to the (100) plane of β-$Ni(OH)_2$ (JCPDS NO. 14-0117), is observed.

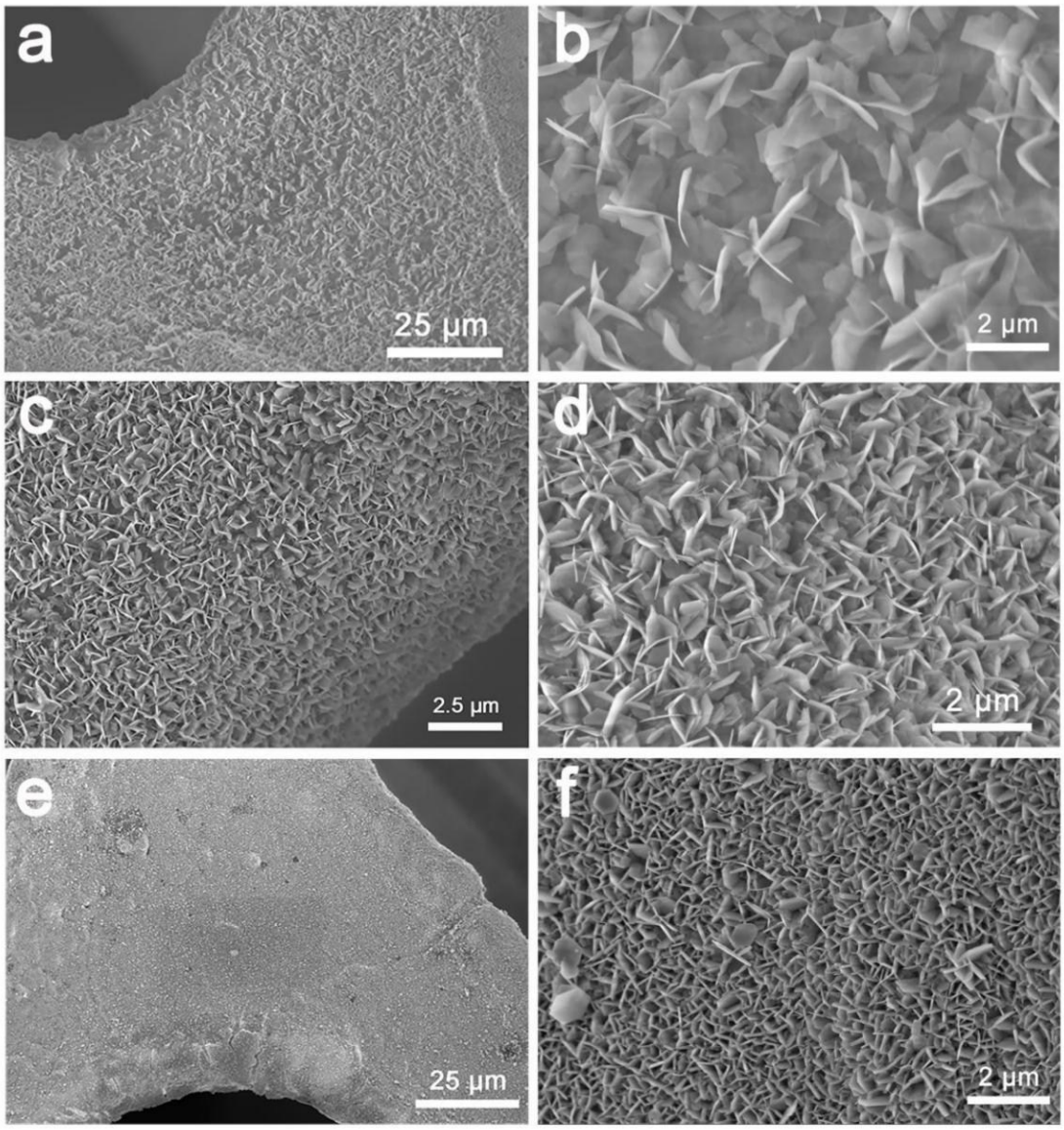

Figure S2. SEM images of act-NF prepared at reaction temperatures of (a and b) 120 ˚C, (c and d) 160 ˚C and (e and f) 200 ˚C, respectively.

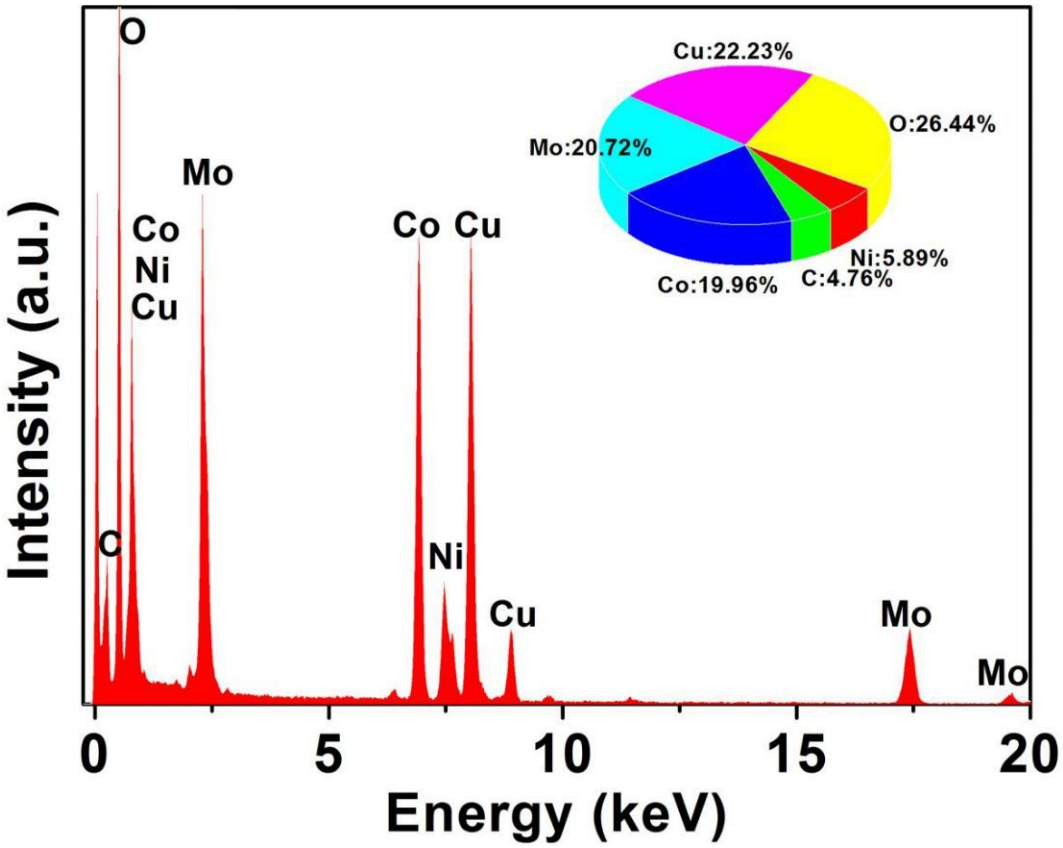

Figure S3. TEM energy dispersive X-ray spectrum (EDS) of $Ni_xCo_{1-x}MoO_4$@$CoMoO_4$ peeled out from NCMO@CMO/act-NF.

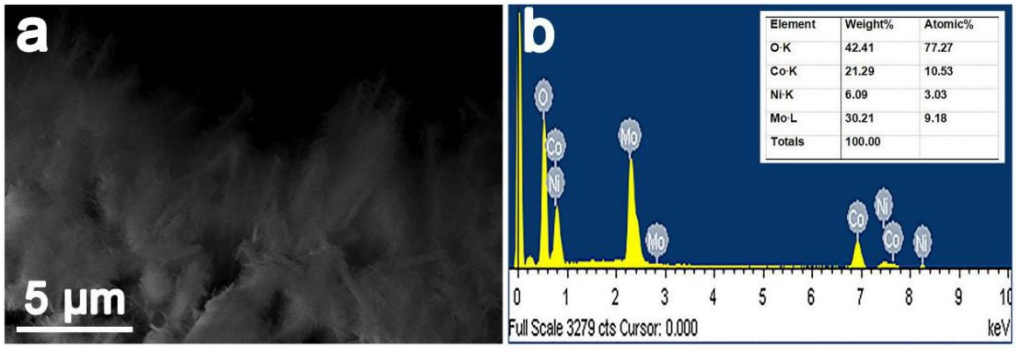

Figure S4. SEM energy dispersive X-ray spectrum (EDS) of NCMO@CMO/act-NF composite electrode.

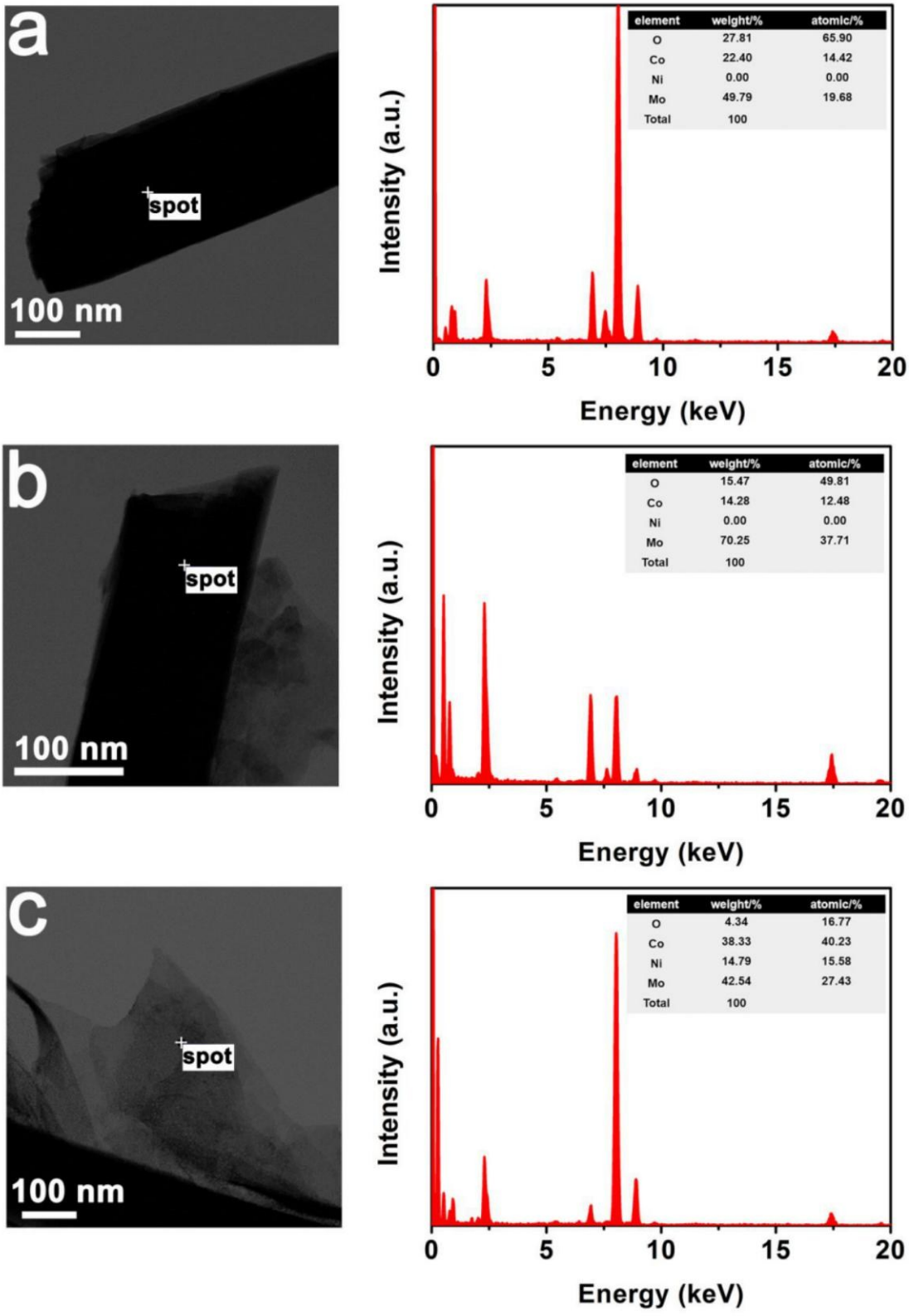
a
spot
100 nm
element weight/% atomic/%
O 27.81 65.90
Co 22.40 14.42
Ni 0.00 0.00
Mo 49.79 19.68
Total 100
Intensity (a.u.)
0 5 10 15 20
Energy (keV)
b
spot
100 nm
element weight/% atomic/%
O 15.47 49.81
Co 14.28 12.48
Ni 0.00 0.00
Mo 70.25 37.71
Total 100
Intensity (a.u.)
0 5 10 15 20
Energy (keV)
c
spot
100 nm
element weight/% atomic/%
O 4.34 16.77
Co 38.33 40.23
Ni 14.79 15.58
Mo 42.54 27.43
Total 100
Intensity (a.u.)
0 5 10 15 20
Energy (keV)

Figure S5. TEM spot energy dispersive X-ray spectrum (EDS) of $CoMoO_4$ nanorod from CMO/NF (a), nanorod parts (b) and nanosheet parts (c) of $Ni_xCo_{1-x}MoO_4$@$CoMoO_4$.

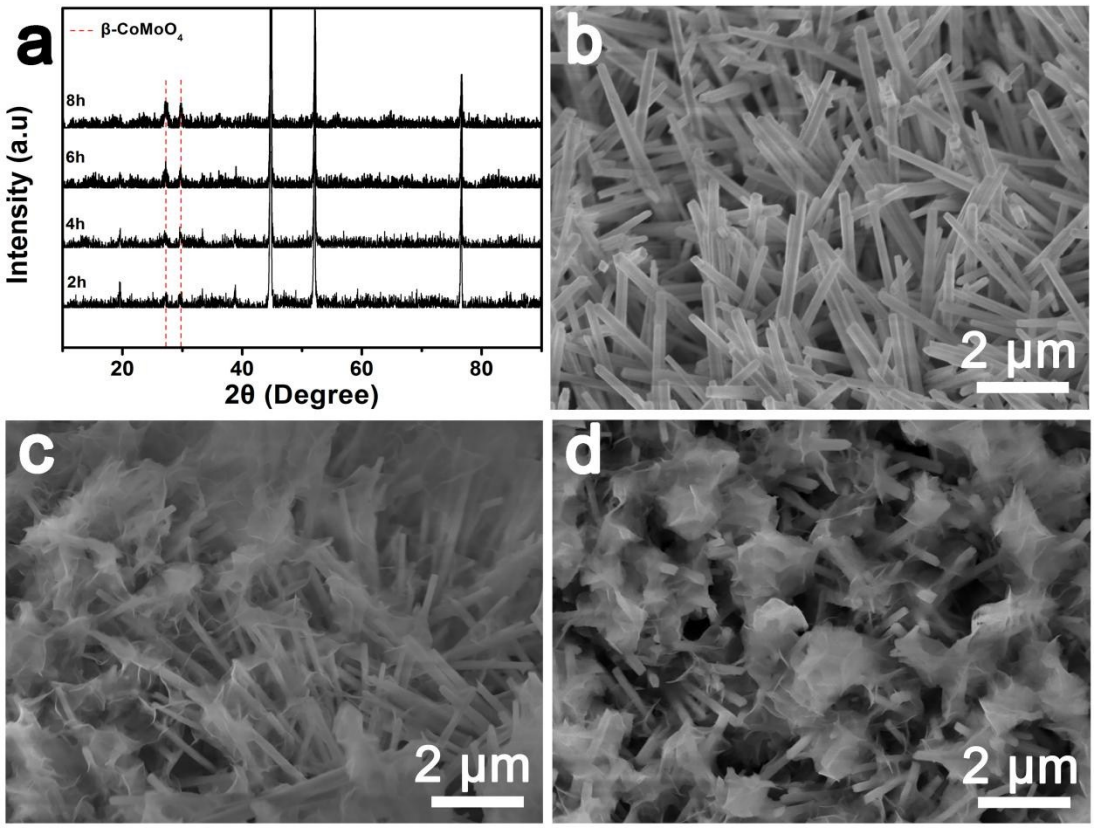

Figure S6. (a) XRD patterns of NCMO@CMO/act-NF with reaction times of 2 h, 4 h, 6 h, and 8 h; SEM images of NCMO@CMO/act-NF with different growth times: (b) 2 h, (c) 4 h, and (d) 6 h, respectively.

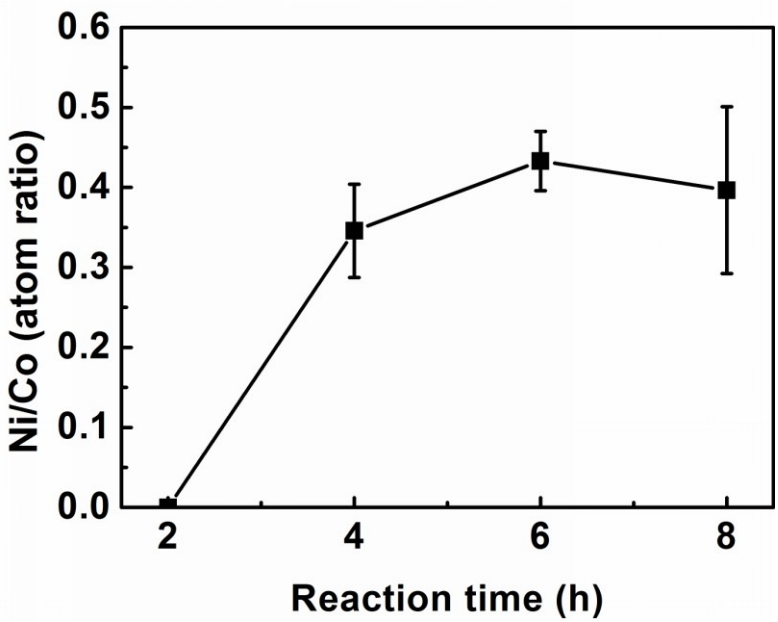

Figure S7. The atomic ratio of Ni/Co selected from EDX for the external $Ni_xCo_{1-x}MoO_4$ growing 2h, 4h, 6h and 8h.

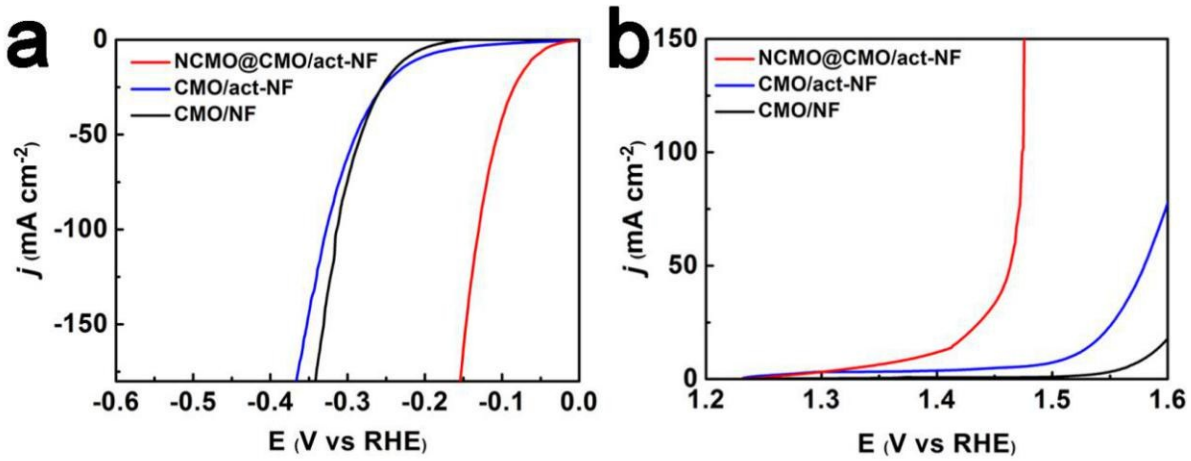

Figure S8. Electrochemical performance of NCMO@CMO/act-NF, CMO/act-NF and CMO/NF for HER (a) and OER (b), respectively.

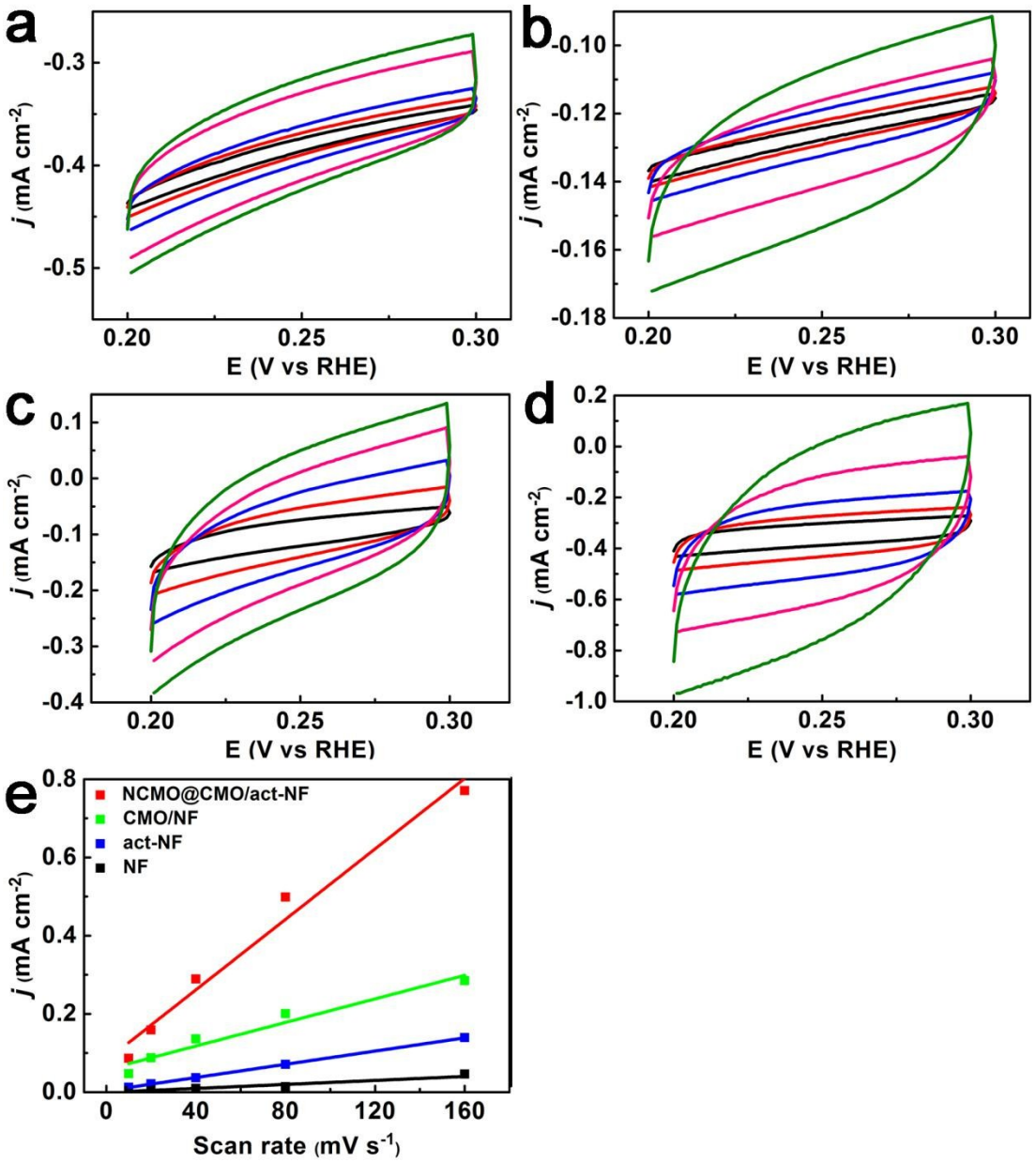

Figure S9. Cyclic voltammograms of (a) NF, (b) act-NF, (c) CMO/NF and (d) NCMO@CMO/act-NF; (e) estimation of C_{dl} by forcing the current density variation [$\Delta j = (j_a - j_c)/2$, at 150 mV vs RHE] versus scan rate to fit linearly.

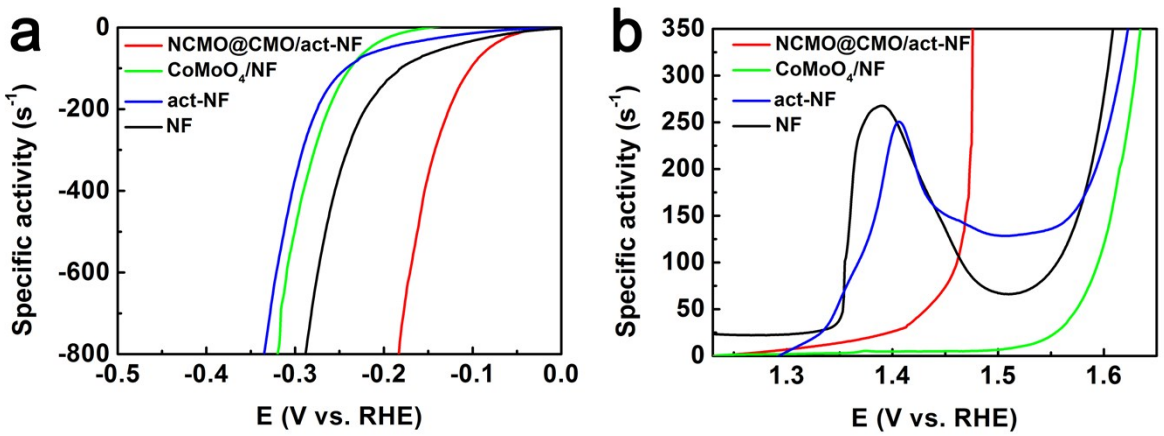

Figure S10. The specific activity of various electrocatalysts in 1M KOH for (a) HER and (b) OER. Data is obtained by dividing the current density by their corresponding Cdl, and further 0.1 V (the voltage range used in CV).

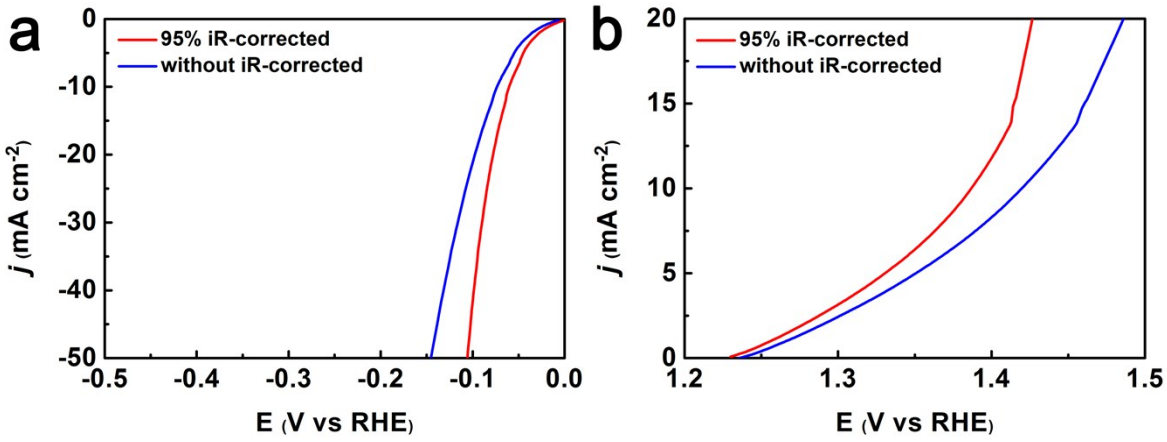

Figure S11. Polarization curves and of NCMO@CMO/act-NF with 95% iR-corrected and without iR-corrected for HER(a) and OER(b), respectively.

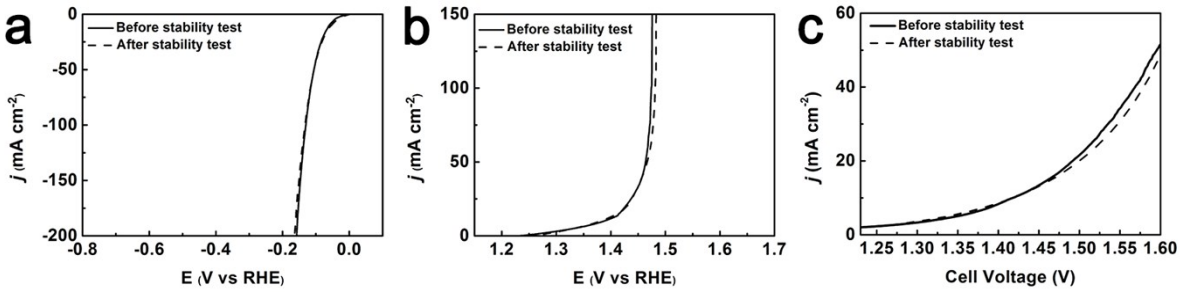

Figure S12. Polarization curves of NCMO@CMO/act-NF before and after stability test for HER(a), OER(b) and overall water splitting(c).

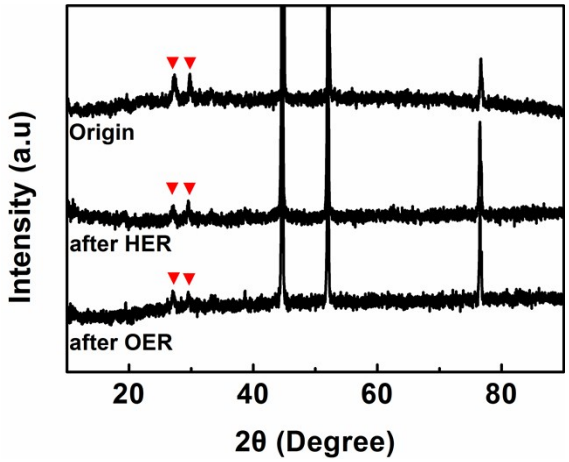

Figure S13. XRD pattern for NCMO@CMO/act-NF and NCMO@CMO/act-NF after HER and OER durability test.

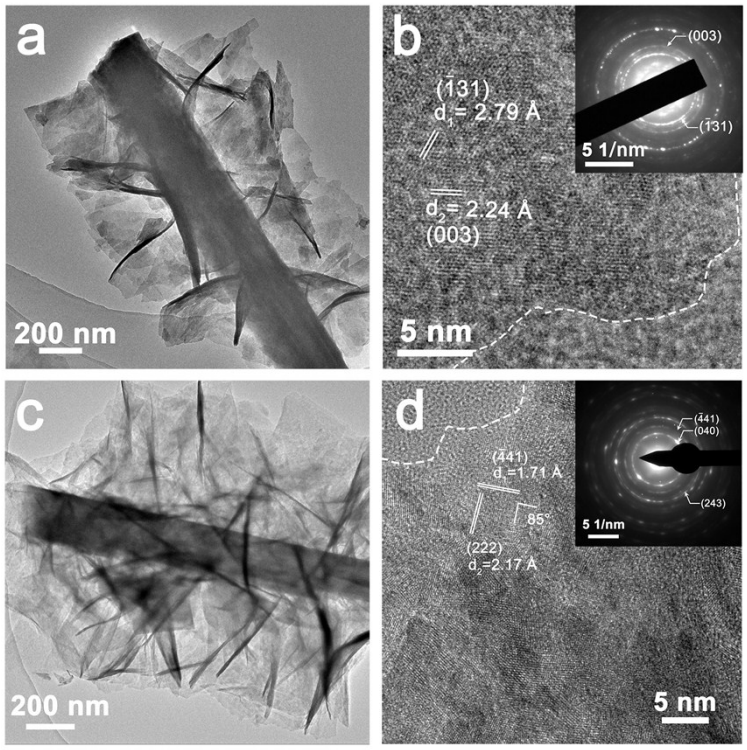

Figure S14. TEM, HRTEM and SAED pattern of $Ni_xCo_{1-x}MoO_4$@$CoMoO_4$ after HER (a, b) durability test and OER durability test (c, d), respectively.

Computational details and models

All calculation were performed in the framework of the periodic density functional theory (DFT) by using code from the Vienna Ab initio Simulation Package (VASP).[1] The exchange correlation potential was described using the Perdew-Burke-Ernzerhof (PBE) functional within the generalized gradient approximation (GGA).[2] The energy cutoff of the plane-wave basis set was chosen to be 300 eV, the convergence criterion for the total energy was set to 1×10^{-5} eV, and that of the force on each atom was set to 0.02 eV/Å. The Monkhorst-Pack scheme *k*-point grids were 2×2×3 for structural optimizations. For electronic structure calculations, the *k*-point values were set to 4×4×6. Spin-polarized calculations were carried out for all the systems.

According to the experimental results, the pristine β-$CoMoO_4$ 1×1×2 supercell containing 96 atoms was used with dimensions of 10.09Å×9.17Å×14.08Å. Substitutional

Ni doping (Ni-$CoMoO_4$) was modeled by replacing a Co atom in the supercell, as **Figure S13 .**

In this paper, the d band centers (ε_d) of the Co and Ni atoms were calculated as follows:

$$\varepsilon_d = \frac{\int_{-\infty}^{+\infty} \rho_d(E) E dE}{\int_{-\infty}^{+\infty} \rho_d(E) E dE}$$

Where ε_d represents the projected density of states of the d orbitals of the metal atom, and E represents the energy with regard to the Fermi level.

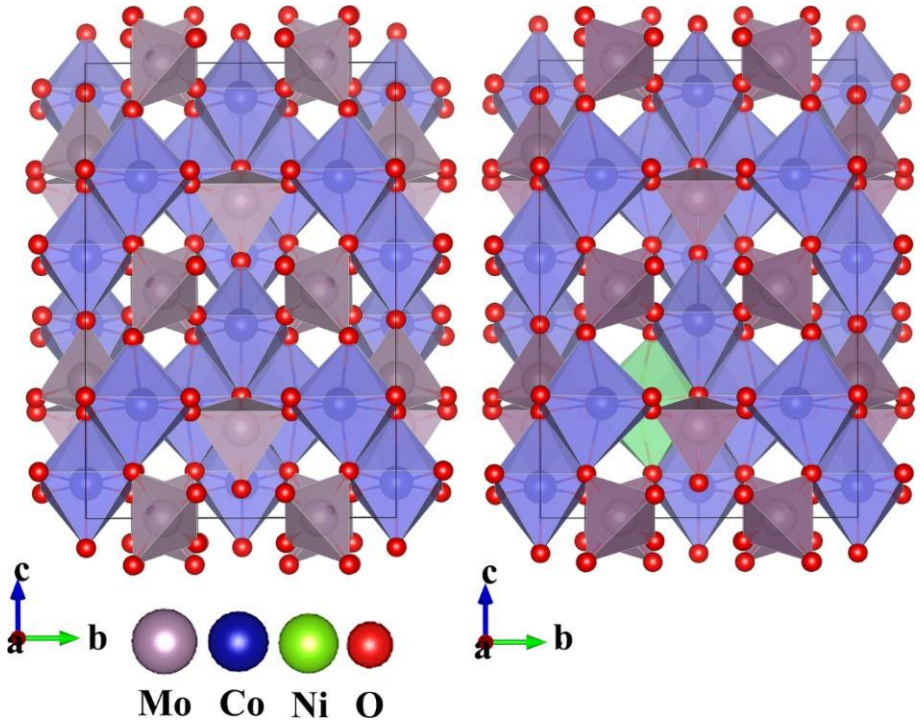

Figure S15. The geometric configuration of $CoMoO_4$ (left) and Ni-$CoMoO_4$ (right) with Ni atom replacing the Co atom.

Table S1. Comparison of the HER performance of NCMO@CMO/act-NF electrode with other reported HER electrocatalysts in basic electrolyte.

Catalyst	Electrolyte	η(mV)@j ($mA\ cm^{-2}$)	Tafel Slope ($mV\ dec^{-1}$)	Reference
$Ni_xCo_{1-x}MoO_4$@$CoMoO_4$	1 M KOH	61	63	This Work
$NiCo_2O_4$	1 M NaOH	110	49.7	[3]
Co–P@Co_3O_4	1 M KOH	73	76	[4]
NiO NRs	1 M KOH	110	100	[5]
Ni-Co-P	1 M KOH	58	57	[6]

Ni/NiP	1 M KOH	130	58.5	[7]
MoS_2/Ni_3S_2	1 M KOH	110	83	[8]
NC-NiCu-NiCuN	1 M KOH	93	55	[9]
Ni_2P/Ni/NF	1 M KOH	98	72	[10]
EG/$Co_{0.85}$Se/NiFe-LDH	1 M KOH	260	NA	[11]
NiFe/$NiCo_2O_4$	1 M KOH	105	88	[12]

Table S2. Comparison of the OER performance of NCMO@CMO/act-NF electrode with other reported OER electrocatalysts in basic electrolyte.

Catalyst	**Electrolyte**	**η(mV)@j ($mA\ cm^{-2}$)**	**Tafel Slope ($mV\ dec^{-1}$)**	**Reference**
$Ni_xCo_{1-x}MoO_4$@$CoMoO_4$	1 M KOH	140	43	**This Work**
$NiCo_2O_4$	1 M NaOH	290	53	[3]

$CoMoO_4$-$NiMoO_4$	2 M KOH	300	68	[13]
$IrNiO_X$	0.05 M H2SO4	280	NA	[14]
Ni-Co-P	1 M KOH	280	NA	[6]
Ni/NiP	1 M KOH	270 mV@30 mA cm^{-2}	73.2	[7]
MoS_2/Ni_3S_2	1 M KOH	218	88	[8]
NC-NiCu-NiCuN	1 M KOH	232	41	[9]
Ni_2P/Ni/NF	1 M KOH	200	NA	[10]
EG/$Co_{0.85}$Se/NiFe-LDH	1 M KOH	270 mV@150 mA cm^{-2}	57	[11]
NiFe/$NiCo_2O_4$	1 M KOH	250	38.8	[12]

Table S3. Comparison of the overall water splitting performance of NCMO@CMO/act-NF electrode with other reported bifuncational electrocatalysts in basic electrolyte.

Catalyst	**Electrolyte**	**Support**	**Overall**	**Reference**

			voltage(V) @10 mA cm^{-2}	
$Ni_xCo_{1-x}MoO_4$@$CoMoO_4$	1 M KOH	Nickel Foam	1.46	**This Work**
$NiCo_2O_4$	1 M NaOH	Nickel Foam	1.65	[3]
NiO NRs	1 M KOH	Carbon Fiber Paper	1.62	[5]
Ni-Co-P	1 M KOH	Glassy Carbon	1.56	[6]
Ni/NiP	1 M KOH	Nickel Foam	1.61	[7]
MoS_2/Ni_3S_2	1 M KOH	Nickel Foam	1.56	[8]
NC-NiCu-NiCuN	1 M KOH	Nickel Foam	1.56	[9]
Ni_2P/Ni/NF	1 M KOH	Nickel Foam	1.49	[10]
EG/$Co_{0.85}Se$/NiFe-LDH	1 M KOH	Graphene Foil	1.67	[11]
NiFe/$NiCo_2O_4$	1 M KOH	Nickel Foam	1.67	[12]

REFERENCES

1 G. Kresse, J. Furthmüller, *Phys. Rev. B,* 1996, **54**, 11169−11186.

2 J. P. Perdew, K. Burke, M. Ernzerhof, *Phys. Rev. Lett.,* 1996, **77**, 3865−3868.

3 X. Gao, H. Zhang, Q. Li, X. Yu, Z. Hong, X. Zhang, Z. Lin, *Angew. Chem. Int. Ed.,* 2016, **128**, 6398-6402.

4 L. Yang, H. Zhou, X. Qin, X. Guo, G. Cui, A. M. Asiri, X. Sun, *Chem. Commun.,* 2018, **54**, 2150-2153.

5 T. Zhang, M. Y. Wu, D. Y. Yan, J. Mao, H. Liu, W. B. Hu, X. W. Du, T. Ling, S. Z. Qiao, *Nano Energy,* 2018, **43**, 103-109.

6 Z. Fang, L. Peng, Y. Qian, X. Zhang, Y. Xie, J. J. Cha, G. Yu, *J. Am. Chem. Soc.,* 2018, **140**, 5241-5247.

7 G. F. Chen, T. Y. Ma, Z. Q. Liu, N. Li, Y. Z. Su, K. Davey, S. Z. Qiao, *Adv. Funct. Mater.,* 2016, **26**, 3314-3323.

8 J. Zhang, T. Wang, D. Pohl, B. Rellinghaus, R. Dong, S. Liu, X. Zhuang, X. Feng, *Angew. Chem. Int. Ed.,* 2016, **55**, 6702-6707.

9 J. Hou, Y. Sun, Z. Li, B. Zhang, S. Cao, Y. Wu, Z. Gao, L. Sun, *Adv. Funct. Mater.,* 2018, **28**, 1803278.

10 B. You, N. Jiang, M. Sheng, M. W. Bhushan, Y. Sun, *ACS Catal.,* 2015, **6**, 714-721.

11 Y. Hou, M. R. Lohe, J. Zhang, S. Liu, X. Zhuang, X. Feng, *Energy Environ. Sci.,* 2016, **9**, 478-483.

12 C. Xiao, Y. Li, X. Lu, C. Zhao, *Adv. Funct. Mater.,* 2016, **26**, 3515-3523.

13 Z. Yin, Y. Chen, Y. Zhao, C. Li, C. Zhu, X. Zhang, *J. Mater. Chem. A,* 2015, **3**, 22750-22758.

14 H. N. Nong, H. S. Oh, T. Reier, E. Willinger, M. G. Willinger, V. Petkov, D.

Teschner, P. Strasser, *Angew. Chem. Int. Ed.,* 2015, **54**, 2975-9.